Copper(II) can kinetically trap Arctic and Italian amyloid-β_{40} as toxic oligomers, mimicking Cu(II) binding to wild-type amyloid-β_{42}: implications for familial Alzheimer's disease

Yao Tian, Qi Shang, Ruina Liang and John H. Viles*

School of Biological and Behavioral Sciences, Queen Mary University of London, London, E1 4NS, United Kingdom

KEYWORDS: Alzheimer's disease; Amyloid; Copper; Kinetics; Molecular Mechanism

ABSTRACT: The self-association of amyloid-β (Aβ) peptide into neurotoxic oligomers is believed to be central to Alzheimer's disease (AD). Copper is known to impact Aβ assembly, while disrupted copper homeostasis impacts phenotype in Alzheimer's models. Here we show the presence of sub-stoichiometric Cu(II) have very different impacts on the assembly of Aβ40 and Aβ42 isoforms. Globally fitting microscopic rate constants for fibril assembly indicates copper will accelerate fibril formation of Aβ40 by increasing primary nucleation, while seeding experiments confirm elongation and secondary nucleation rates are unaffected by Cu(II). In marked contrast, Cu(II) traps Aβ42 as prefibrillar oligomers and curvilinear protofibrils. Remarkably, Cu(II) addition to preformed Aβ42 fibrils causes disassembly of fibrils back to protofibrils and oligomers. The very different behaviors of the two Aβ isoforms are centered around differences in their fibril structures as highlighted by studies of C-terminally amidated Aβ42. Arctic and Italian familiar mutations also support a key role for fibril structure in the interplay of Cu(II) with Aβ40/42 isoforms. The Cu(II) dependent switch in behavior between non-pathogenic Aβ40 wild-type and Aβ40 Arctic or Italian mutants suggests heightened neurotoxicity may be linked to the impact of physiological Cu(II), which traps these familial mutants as oligomers and curvilinear protofibrils, which cause membrane permeability and Ca(II) cellular influx.

INTRODUCTION

Alzheimer's disease (AD) is responsible for the majority of dementias, and worldwide it is estimated 50 million people are currently suffering from this neurogenerative disease.[1] AD pathology is dominated by the accumulation of a small peptide, amyloid-β (Aβ), that forms fibrils.[2-3] These accumulate to form extracellular plaques which also contains phospholipids and metal ions. Rare point-mutations within Aβ such as the Arctic and Italian mutations cause early onset AD and have made a persuasive argument for the amyloid cascade hypothesis, which places Aβ self-association central to AD pathology.[4] Aβ varies in length, with N- and C-terminal extensions and truncations, but is typically 40 and 42 amino acids long.[5] Other genetic mutations, also associated with early onset Alzheimer's disease, cause an increase in Aβ42 production relative to Aβ40.[6-8] In addition, Aβ42 has a greater propensity to form fibrils and plaques which has focused attention on Aβ42 as the toxic Aβ isoform. Small diffusible pre-fibrilar assemblies of Aβ42 are the most synaptotoxic.[9-14] In contrast to fibrils, these oligomeric and extended curvilinear protofibrils are cytotoxic and can carpet the lipid membrane surface,[15] and form ion-channel pores,[16] which cause membrane permeability and a loss of cellular homeostasis.[17]

Potentially, metal ion binding such as Cu(II) and Zn(II) can influence Aβ synaptic toxicity by accelerating fibril formation or promoting pre-fibrillar toxic oligomers.[18-20] While the redox properties of copper ions can produce reactive oxygen species causing oxidative stress observed in AD.[21-22] Copper homeostasis is disrupted in AD patients.[23] Levels of labile copper are found elevated, but only in the most effected regions of the AD brain,[24] and also in blood plasma.[25] The copper ions are concentrated in senile plaques directly bound to Aβ,[26-28] with a four-fold increase in the levels of Cu(II) in the neuropil. Furthermore, heightened Alzheimer's disease phenotypes in both drosophila[29-30] and rabbit models[31] are linked to disrupted copper homeostasis. Additionally, an unbiased screen of 140,000 compounds has shown that copper chealtors, such as Clioquinol, ameliorate Aβ toxicity in a yeast model for Alzheimer's disease.[32] Futhuremore, clioquinol can improve AD phenotypes in mice models,[33] although this has not been replicated in human trials.[34]

Both Aβ40 and Aβ42 binds to Cu(II) with the same picomolar affinity (conditional K_d = 54 pM at pH 7.4) and 1:1 stoichiometry.[35] Thus *in vivo* Aβ (at *ca.* 0.5 nM at the synapse [36]) is expected to compete for Cu(II) which is thought to be released from the synapse at much higher levels, 15 - 250 μM, within the synaptic cleft, especially during depolarisation.[37-38] Weaker Cu-Aβ dissociation constants have been reported, but these are determined in the presence of Cu(II) competitive buffers (such as Tris and phosphate buffer) that reduce the apparent affinity for Cu(II), when a correction is made for this, similar picomolar conditional dissociation constants are calculated. [39]

A large array of approaches have revealed that Cu(II) forms a tetragonal complex with Aβ, containing two nitrogen and two oxygen ligands in the equatorial plain.[35, 40-41] While Cu(II) binds to Aβ40 or Aβ42 with the same coordination geometry.[35] The copper complex involves the N-terminal third of Aβ, indeed there is no difference in the Cu(II) complex formed with Aβ(1-16) compared to Aβ40 and Aβ42.[35, 39, 41] The complex is dynamic and forms a number of interchangeable ligands which include two of the three histidine imidazole nitrogen's (His6; His13; His14) along with carboxyl coordination (e.g. Asp1, Asp7, Glu11).[35, 42-44] Solid-state nuclear magnetic resonance (NMR) and pulsed electron paramagnetic resonance (EPR) spectroscopy of the Cu^{2+} complex indicates that the fibrillar form of Aβ40 can accommodate Cu^{2+} coordination.[45-46]

The impact Cu(II) has on Aβ40 and Aβ42 fibril assembly has been peppered with conflicting reports; both acceleration and inhibition of fibril formation has been reported. Much of the conflicting observations can be accounted for by differing experimental conditions. Furthermore, in the early studies little distinction was made between amorphous aggregation, amyloid formation and pre-fibrillar oligomer formation. It is now established, supra-stoichiometric amounts of Cu(II) bound to Aβ tends to promote amorphous aggregates but not ordered amyloids, as the second copper ion bound causes Aβ to become insoluble.[47] Sub-stoichiometric levels of Cu(II) binding to Aβ is more representative of Cu(II) loading on Aβ *in vivo*, and affects Aβ quite differently. In the case of Aβ42, most studies report sub-stoichiometric amounts of Cu(II) inhibit fibril formation.[48-50] Here, we will show Cu(II) actually traps Aβ as pre-fibral oligomers, which upon the removal of Cu(II) will nucleate (or seed) fibril formation. The impact of fibril formation with sub-stoichiometric addition of Cu(II) to Aβ40 remains poorly established with conflicting observations. Some studies report Cu(II) to accelerate Aβ40 fibril formation,[22, 47-48, 51] but this is not universally reported.[52-53] In addition, there are now studies that have focused on Cu(II)-Aβ interactions for various point mutations, these include Iowa (D23N), A2V, and D7H, which are linked to inherited AD.[54-56]

Like Cu(II), Zn(II) also binds to Aβ via histidines and carboxylate coordination, forming a dynamic, rapidly exchanging complex. [39, 57-59, 60, 61] Trace levels of Zn(II) (0.01 mole equivalents) profoundly influences fibril assembly by rapidly exchanging between Aβ peptides.[62]

It is assumed that Aβ42 heightened neurotoxicity relative to Aβ40, is associated with heightened oligomer and fibril formation. Here we show a marked difference in the way Cu(II) influences assembly of non-pathogenic Aβ40 compared to pathogenic Aβ42. In particular, sub-stoichiometric Cu(II) can trap Aβ42 in an oligomeric form but not Aβ40. We wondered if early onset AD, caused by point mutations such as Arctic an Italian Aβ40 mutations, are also influenced differently by Cu(II) compared to the wild-type Aβ40. Here we revisit copper's impact on fibrilization for both Aβ40 and Aβ42, by globally fitting the kinetic fibril growth curves to individual microscopic rate constants, so as to understand the mechanism behind the switch in impact of Cu(II), as a promoter and inhibitor of fibril formation. With the identical copper coordination geometry for Aβ40 and Aβ42, the switch in behavior might be accounted for by the very different fibril structures, which form 'U' and 'S' shaped fibrils, for of Aβ40 and Aβ42 respectively, Figure S1. The difference in structure is caused by columbic interactions between the Lys28 amino group and the carboxylate at Asp23 or the C- terminal carboxylate at Ala42, Figure S1. To probe this question, we have explored a series of Aβ analogues including, the C-terminally amidated and N-terminally acetylated Aβ, together with familiar mutants, the Arctic(D22G) and Italian(D22K) for Aβ40 and Aβ42 familial isoforms. This has helped us understand how different Aβ isoforms, and their associated tendency to form different fibril structures, are impacted by Cu(II).

RESULTS AND DISCUSSION

Contrasting influence of Cu(II) on the kinetics of fibril assembly for Aβ40 and Aβ42

First we wanted to determine the influence of sub-stoichiometric Cu(II) on the kinetics and structure of both wild-type Aβ40 and Aβ42 fibril formation. Although this has been the subject of interest for several years, the influence of Cu(II) on Aβ40/42 assembly still remains disputed.[22, 47-53] Figure. 1A, shows the kinetics of Aβ40 as monitored by the amyloid specific dye Thioflavin T (ThT). Increasing levels of Cu(II) causes, accelerated fibril formation kinetics with a significant shortening of lag-times from a mean of 56.0 ± 0.9 hrs for Aβ40 in the absence of Cu(II) to 24.9 ± 0.8 hrs for Cu-Aβ40 at 1:1 stoichiometric loading, as summarized in Figure 1C and Table S1.

It has been suggested that Cu(II) might interfere with the ability of ThT to detect fibrils by quenching the ThT fluorescence, however, we observe no evidence of this. The ThT kinetic traces, shown in Figure 1A, are for absolute ThT intensity, and are not normalized. Cu(II) does not impact the ability to detect fibrils of Aβ40, and there is no change in the total ThT signal, Figure 1A, S2A and Table S1. This is supported by TEM images, Figure 1D and Figure S3, that show a similar abundance of fibrils for both Cu(II) loaded and Cu(II) free Aβ40.

Next, we performed a similar ThT monitored fibril assembly experiment on the more neurotoxic Aβ42, Figure 1B. Cu(II) has a starkly different impact on the fibril assembly for Aβ42; rather than acceleration of fibril assembly, the amount and rate of fibril formation is greatly reduced. Cu(II) at just 0.5 mole equivalent reduces the ThT signal by more than two-thirds, Figure S2B, while Cu(II) at 1:1 reduces the ThT signal intensity even more to just 11%, while the rate of fibril formation is extended with t_{50} going from 35.6 ± 1.1 hrs to 67.3 ± 0.3 hrs, see Figure 1C and Table S1. The marked reduction in the total number of fibrils indicated by the ThT signal is supported by TEM images, that show almost no fibrils present for images of Aβ42 incubated with 0.5 mole equivalent of Cu(II), see Figure 1E and Figure S4. Quantification of the total fibril load from the TEM micrographs match the marked drop in ThT signal with an 84% reduction in of the number of fibrils present in the Cu(II) loaded sample (n=50 images inspected). Instead, many pre-fibril assemblies are observed; short oligomers and more extended curvilinear protofibrils, but almost no fibrils, Figure 1E and Figure S4.

We wondered if the conflicting behavior reported indicating Cu(II) inhibition of Aβ40 fibril formation rather than acceleration [52-53], was due to differences in experimental conditions, particularly the use of phosphate buffer, which can form insoluble Cu(II)-phosphate. However, the presence of phosphate buffer, in our study, did not alter the impact of Cu(II) on Aβ40 assembly, and like the data in Figure 1A, Aβ40 fibril formation is accelerated by Cu(II) addition, up to 1 mole equivalent, see Figure S5. Furthermore, the acceleration of Aβ40 by Cu(II) has been reported by others,[22, 47-48, 51] thus the difference in the reported influence of Cu(II) on Aβ40 fibril formation kinetics is quite surprising and is difficult to account for.

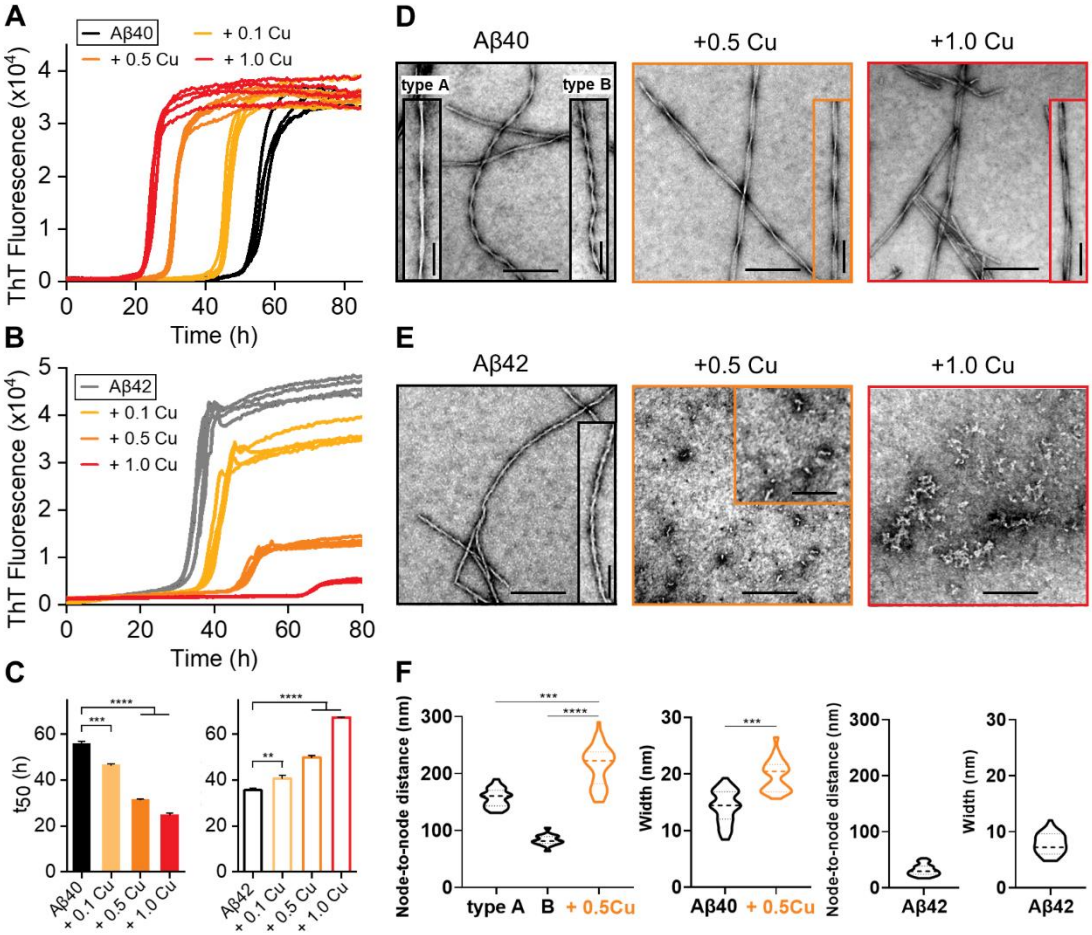

Figure 1: The effect of Cu^{2+} on Aβ40 and Aβ42 fibril kinetics profiles. Aβ40 (A) and Aβ42 (B) both 10 μM in the absence and presence of 0.1, 0.5 and 1.0 molar equivalents of Cu^{2+}, from black line to red line respectively. (C) Change in t_{50} versus Cu^{2+}, error bars are standard error of the mean (SEM) from four replicates. One-way ANOVA test, **P ≤ 0.01, ***P ≤ 0.001, ****P ≤ 0.0001. Negatively stained TEM fibril images produced at 0, 0.5 and 1.0 molar equivalents of Cu^{2+} for Aβ40 (D) and Aβ42 (E). Scale bars: 200 nm; inset 100 nm. (F) Node-to-node distance of Aβ40 and Aβ42 fibril twists and fibril width in the absence and presence of 0.5 molar equivalents of Cu^{2+}. N=50 individual fibrils are measured per condition. Long and short twist are designated type A and B respectively. Preparations were incubated with 20 μM ThT in 30 mM HEPES and 160 mM NaCl buffer (pH 7.4) at 30 °C quiescently.

The different impact of Cu(II) on the structure of Aβ40 and Aβ42 assemblies

Amyloid fibrils are well known for their ability to form polymorphic structures.[63-64] The TEM images suggest copper-free Aβ40 have two distinct fibril morphologies, even when generated from size exclusion chromatography (SEC) purified Aβ40 monomer. The node-to-node periodicity in the twist are 157 ± 16 nm (designated type-A), and 83 ± 1 nm (type-B) shown in Figure 1F. When Aβ40 is incubated with Cu(II), copper binding directs the type of fibrils produced into a single morphology type, similar to type-A with the longer twist of 242 ± 50 nm. The fibril morphology is typically determined by the way protofibrils packed together to form a twisting fibril.[63-64] This suggests the presence of Cu(II) restricts the type of protofibril packing possible, this mechanism is illustrated in Figure S6.

As already shown in Figure 1E, almost no fibrils of Aβ42 are observed when Cu(II) is incubated with Aβ42, however there are many prefibrillar assemblies observed, further images are shown in Figure 2 and Figure S4. Small oligomers and extended oligomers, known as curvilinear protofibrils, are widespread. These assemblies have been subject to single particle analysis of the negatively stained images, typical 2D class-averages are shown in Figure 2C. These pre-fibrillar assemblies are indistinguishable from the oligomers and curvilinear protofibrils but only transiently observed during copper free assembly at the end of the lag-time.

It is well established that oligomers and the curvilinear protofibrils are the cytotoxic form of Aβ, rather than fibrils.[11, 14, 65-66] The influence of the Cu(II) promoted oligomers on membrane permeability, Ca(II) cellular influx and cytotoxicity is described later.

Micro-rate constants, copper's impact on primary nucleation

To understand the mechanism of this acceleration and retardation of Aβ40 and Aβ42 fibril formation, we have globally fitted, the ThT kinetic data to a set of analytical rate equations [67]. This has enabled us to determine in what way Cu(II) impacts the individual microscopic molecular processes of assembly. The macroscopic kinetic curves are described in terms of primary nucleation (k_n), secondary nucleation (k_2), and elongation rates (k_+), using the online fitting program, AmyloFit.[67] Figure 3A shows a good fit to the kinetic data in which only primary nucleation (k_n) is

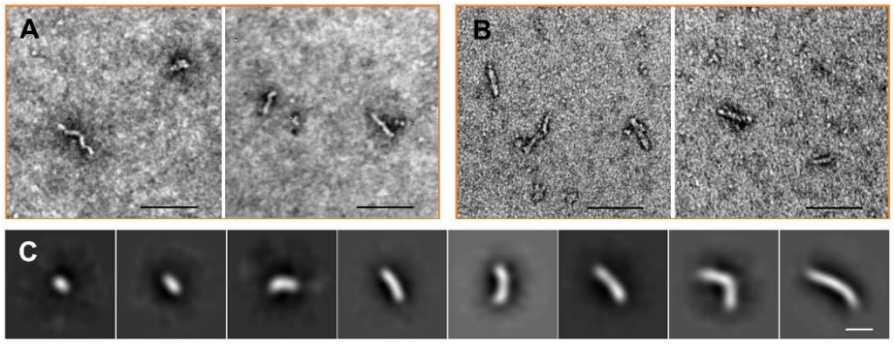

Figure 2: TEM images of Cu^{2+} trapped Aβ42 oligomers. (A) TEM images of 10 μM Aβ42 incubated with 5 μM Cu(II). (B) TEM images of oligomers from preformed fibrils with subsequent addition of Cu(II), scale bars: 200 nm. (C) 2D class averages of oligomers and curvilinear protofibrils for Aβ42 trapped by Cu(II), *ca.* 100 single particles are shown for each 2D class average, scale bar 5 nm.

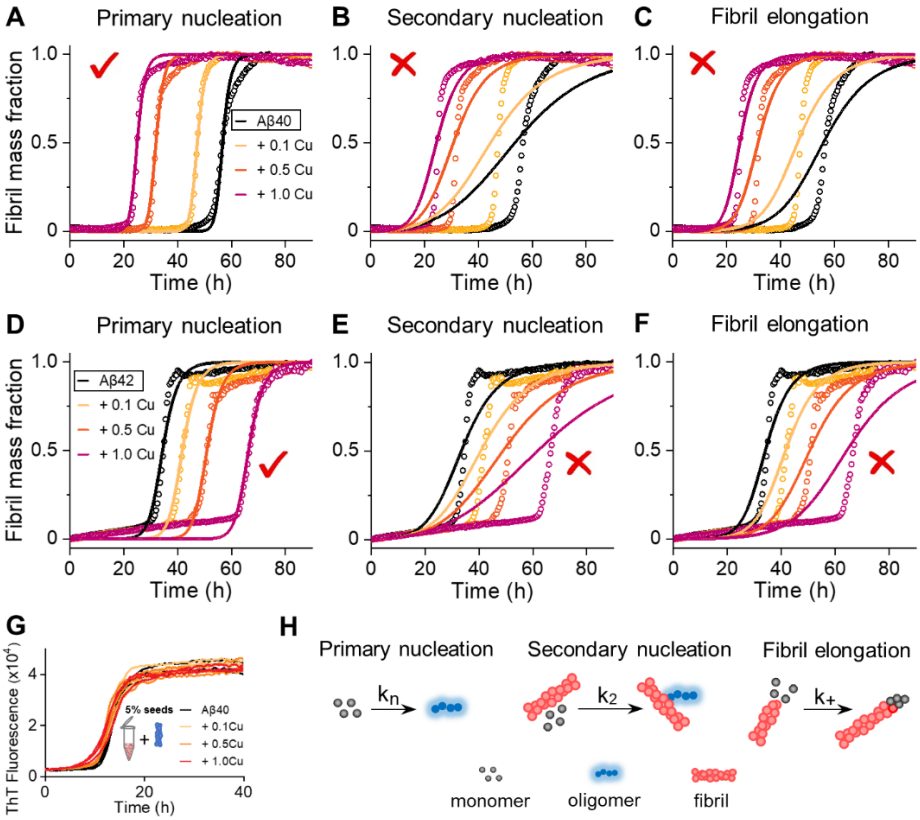

Figure 3: Cu^{2+} effects primary nucleation process of Aβ40 and Aβ42 aggregation. Normalized kinetic profiles of 10 μM Aβ40 (A-C) and Aβ42 (D-E) in the absence and presence of 0.1, 0.5 and 1.0 molar equivalents of Cu^{2+}, from black line to red line respectively. The solid lines represent global fits of the kinetic traces when only primary nucleation (k_n) (A, D), secondary nucleation (k_2) (B, E) and fibril elongation (k_+) (C, F) rate constants are altered. (G) Aβ40 with 5% fibril seeds in the absence and presence of 0.1, 0.5 and 1.0 molar equivalents of Cu^{2+}. (H) Schemes of the microscopic steps for primary nucleation, secondary nucleation, and fibril elongation.

permitted to vary with increasing Cu(II) addition to Aβ40, while k_2 and k_+ are fixed at a single value by globally fitting these rate constants. In contrast, if k_n is fitted to a single value and the secondary nucleation or elongation rate constants are permitted to vary, a fit to the set of macroscopic fibril formation curves is not achieved, Figure 3B and 3C. These globally fitted traces indicate Cu(II) only accelerates Aβ40 fibril formation via a change in primary nucleation (k_n). To support this assertion, we generated ThT kinetic traces seeded with 5% fibrils, this has the effect of circumventing primary nucleation (k_n). These seeded fibril growth curves are unaffected by the presence of Cu(II), Figure 3G. This confirms coppers impact of Aβ40 fibril assembly is dominated by changes in primary nucleation and has little impact on k_2 and k_+.

The acceleration in fibril formation via primary nucleation can be explained by Cu(II) adding positive charge to Aβ. At physiological pH 7.4, Aβ's histidine residues are largely deprotonated, thus the binding of copper adds two positive charges. Aβ has a pI of 5.3, so Cu(II) binding makes Aβ more neutrally charged and more prone to self-association and fibril formation. We have recently reported a similar acceleration of primary nucleation as positive charge, in the form of protons, is added to Aβ by lowering the pH. Like Cu(II) addition, the change in pH also only accelerates primary nucleation.[68]

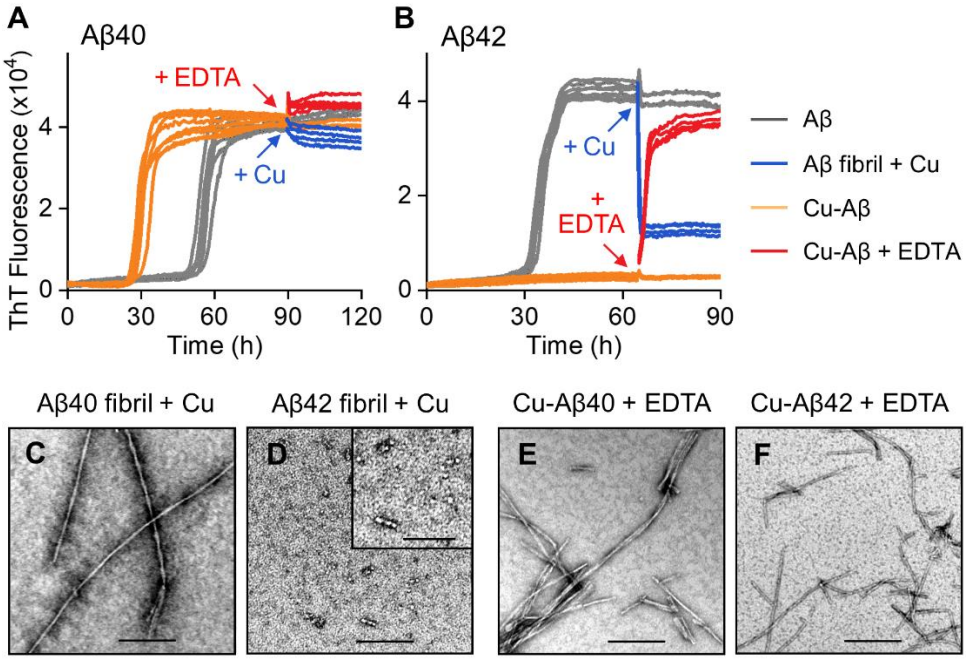

Figure 4: Switching on/off the fibril growth of Aβ by EDTA and Cu^{2+}. Kinetics profiles of 10 μM Aβ40 (A) and Aβ42 (B) in the absence (gray) and presence (orange) of 8 μM Cu^{2+}. 8 μM Cu^{2+} (blue) or 50 μM EDTA (red) was added to half the samples at 90 h for Aβ40 and 65 h for Aβ42. N = 4 traces for each condition. TEM images of Aβ40 (C) and Aβ42 (D) produced with Cu^{2+} added to preformed fibrils. Aβ40 (E) and Aβ42 (F) in the presence of Cu^{2+} with subsequent EDTA addition. Scale bars: 200 nm; inset 100 nm.

Fibril growth curves for Aβ42 have also been fitted to individual microscopic rate constants, in the presence of increasing Cu(II). Cu(II) has a very different effect on Aβ42 assembly compared to Aβ40. The reduction in fibril growth rates with Cu(II) addition appears to be caused by a reduction in primary nucleation. The reduction in the rate of fibril formation and the loss of total fibril mass, could be due to the removal of available Aβ42 monomers capable of forming fibrils, however, the change in lag-time could also be caused by a change in the rate of fibril dis-assembly. The following section makes it clear that Cu(II) can dissociate preformed Aβ42 fibrils. The molecular process associated with Cu(II) mediated Aβ42 assembly/disassembly are discussed further in the following section.

Cu(II) induced disassembly of Aβ42 fibrils: EDTA chelator and Cu(II) addition to preformed fibrils

To further probe the Cu(II) dependent effects on fibril assembly we used a tight Cu(II) chelator, EDTA, to remove Cu(II) from Aβ, Figure 4. While in the reverse experiment Cu(II) has been added to preformed fibrils, Figure 4. As expected, from Figure 1A, the addition of Cu(II) to preformed Aβ40 fibrils had no significant effect on the ThT fibril signal. Similarly, addition of EDTA to copper loaded Aβ40 fibrils had no impact on the total amount of fibrils. This also confirms Cu(II) does not quench the ThT signal. The effect EDTA has on Cu-Aβ42 is very different. Upon the addition of EDTA, the ThT fluorescence signal for fibrils rapidly increases and reaches a ThT intensity comparable to the Aβ42 in the absence of Cu(II). There are two important observations to note about this behaviour. The inhibitory effect of Cu(II) on Aβ42 fibril formation is completely reversible with the removal of Cu(II) by EDTA. Also, upon removal of Cu(II), Aβ42 fibrils form very rapidly. The lag-time to fibril formation is reduced from 32 hours to just 0.8 hrs, and the t_{50} is just 3.2 hrs after addition of EDTA. This indicates the Cu(II)-trapped, oligomers and curvilinear protofibrils are able to, nucleate (seed) fibril formation. The growth time (slope) is similar for the seeded fibril formation, this indicates the seeds impact primary nucleation (the lag-time), rather than secondary nucleation and elongation (the growth-time) which require fibrils to be present as well as monomer.

Most surprising is the marked effect upon the addition of Cu(II) to preformed Aβ42 fibrils. Despite the well documented stability of fibrils, the addition of Cu(II) to Aβ42, but not Aβ40 fibrils, causes rapid dis-assembly of amyloid fibrils, Figure 4. The effect has incorrectly been interpreted as Cu(II) interfering with the detection of fibrils by ThT, however, the complete loss of fibrils, imaged by TEM, confirms Cu(II) efficiently disaggregates amyloid fibrils of Aβ42 (but not Aβ40), Figure 4C-E. The observation that Cu(II) is able to dis-assemble pre-formed Aβ42 fibrils indicates that the mechanism of inhibition is not removing an available pool of Aβ42 monomer; the action of Cu(II) involves the reversal of fibril assembly. Cu(II) does not just slow fibril formation but to a large extent can reverse and disassemble preformed fibrils. These observations (Figure 4) together with the microscopic kinetic analysis (Figure 3) can lead us to a scheme of fibril assembly behavior in the presence of Cu(II), as shown in Figure 5. We suggest that Cu(II) disrupts the packing between protofibrils and dis-assembles fibrils back to curvilinear protofibrils. The stability of fibrils due to hydrogen-bonding in a cross-β structure is well documented, while the action of Cu(II) is between protofibrils, which are only formed from electrostatic and hydrophobic interactions and not via regular hydrogen-bonding, see Figure 5.

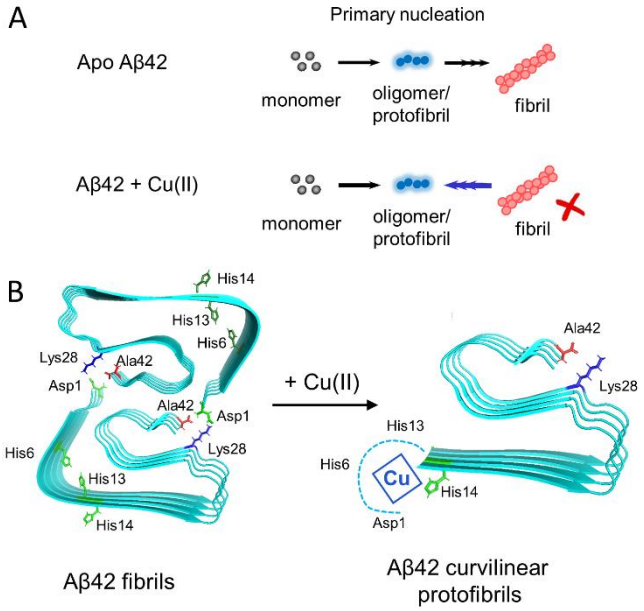

Figure 5: Scheme of Cu(II)'s impact on Aβ42 fibrilization. (A) Primary Nucleation; the kinetic steps to go from monomer to fibrils, in which oligomer formation is the rate-limiting step. Addition of Cu(II) causes Aβ42 to dissociate from fibril to form protofibrils. (B) Aβ42 fibrils are formed from the packing of two protofibrils. Key residues in the N-terminus bind Cu(II) and disrupt the electrostatic packing of protofibrils causing the fibrils to dissociate. Fibril structure from pdb 5OQV.[71]

Cu(II) promoted Aβ cytotoxicity and cellular membrane permeability

Aβ cytotoxicity is believed to be caused by membrane permeability, this results in unregulated Ca(II) cellular influx into the lumen.[9-14, 17, 43] The Ca(II) sensitive fluorescent dye Fluro3-AM has therefore been used to monitor cellular membrane permeability in the presence of different forms of Aβ42, Figure 6. Figure 6A highlights five different Aβ42 preparations used, from various stages of fibril formation. Chromatographic purified monomeric Aβ42, added to the extracellular medium (5 μM) has no effect on Ca(II) levels within the cell lumen, Figure 6B. Similarly Aβ42 fibrils, taken at the plateau phase of fibril growth, have no impact on cellular Ca(II) levels, also shown in Figure 6B. While in contrast, oligomers of Aβ42, taken at the end of the lag-phase, cause considerable Ca(II) influx, within a minute after exposure to the cell, Figure 6B. Importantly, oligomeric preparations, produced by disassembly of Aβ42 fibrils induced by Cu(II) addition, are also capable of causing considerable membrane permeability and Ca(II) cellular influx, Figure 6C. In addition, a preparation in which Cu(II) traps Aβ42 as oligomers, (preparations that would otherwise have formed fibrils) also cause profound membrane permeability, Figure 6E.

The ability for Cu(II) to trap Aβ42 into toxic oligomeric assemblies, or convert Aβ42 fibrils into toxic oligomers, has a profound implication for copper's impact on Aβ42 cytotoxicity. *In vivo*, heightened neurotoxicity of Aβ42, relative to Aβ40, could conceivably be due to the difference in the way physiological Cu(II) impacts Aβ assembly; trapping only Aβ42 as toxic oligomers.

The differential effects of Cu(II) on Aβ40 and Aβ42 fibril formation, probed with a C-terminal amidated analogue

We were intrigued by the very different impact Cu(II) has on the assembly and disassembly of amyloid fibrils for Aβ40 compared to pathogenic Aβ42. It is very well established that Cu(II) binds to these isoforms with the same coordination geometry and affinity; forming an interchangeable (2N2O) tetragonal complex with two of the three histidines (His6; His13; or His14) and carboxylates (eg. Asp1; Asp7 or Glu11).[35, 40-44] This suggests the differences must be associated with the structure of fibrils formed, rather than a difference in Cu(II) coordination. There are now several structures reported for Aβ40 and Aβ42 determined by cryoEM and solid-state NMR.[69-74]

An interesting consequence of the addition of two amino acids at the C- terminus of Aβ42 is the ability for the C-terminal carboxylate to form coulombic interactions with the amino group of Lys28.[69-70] This interaction is not typically favored for the C-terminus of Aβ40 fibrils, instead the salt-bridge occurs between Lys28 and Asp23, see Figure S1. A consequence, of the 'S' shaped arrangement, reported in both recombinant fibrils and brain derived Aβ42 fibril structures[71, 74] is a role for the N-terminal residues which typically form part of the protofibril interface, see Figure 5. While for Aβ40 fibrils the Cu(II) binding N-terminal residues remain unstructured in the fibrils,[70] thus the N-terminal residues seem less necessary for the protofibril interface, Figure S6.

To test the importance of the C-terminal carboxylate in forming a coulombic interaction with Lys28, we studied a C-terminally amidated analogue of Aβ42, which is unable to form a columbic interaction with Lys28 amino group. The C-terminally blocked analogue switches the impact of Cu(II) on Aβ42 assembly, in contrast to wild-type Aβ42, Cu(II) does not trap $Aβ42_{C\text{-}blocked}$ as oligomers, as indicated by the strong ThT signal produces as fibrils form, Figure 7A. This is apparent from the ThT kinetic curves, Figure 7A and TEM images, Figure 7C and further images Figure S7. The effect of Cu(II) addition to performed fibrils and the impact of EDTA on the Cu-loaded fibrils, has also been studied and confirms Cu(II) does not disassemble $Aβ42_{C\text{-}blocked}$ fibrils, Figure 7B and TEM images (Figure 7G and Figure S7) as compared to the behavior wild-type Aβ42 shown in Figure 4. This strongly supports the assertion that the different behavior of Aβ40 compared to Aβ42, are indeed produced by the difference in the fundamental fold of the fibril structures, which is caused by the presence of Ala42 carboxylate salt-bridge. Support for this switch in fibril structure for the $Aβ42_{C\text{-}blocked}$ analogue, is derived from cross-seeding experiments,[75] which indicate the two fibril structures are sufficiently different to be incompatible and do not cross-seed during fibril formation.

The impact on the N-terminal acetylated analogue for Aβ42 was also studied, Figure 7D-F and Figure S8. In this case there is no difference in the fibril assembly compared to wild-type Aβ42. This indicates that acetylation of the N-terminal amino group does not disrupt the manner in which Cu(II) traps Aβ42 assembly as oligomers.

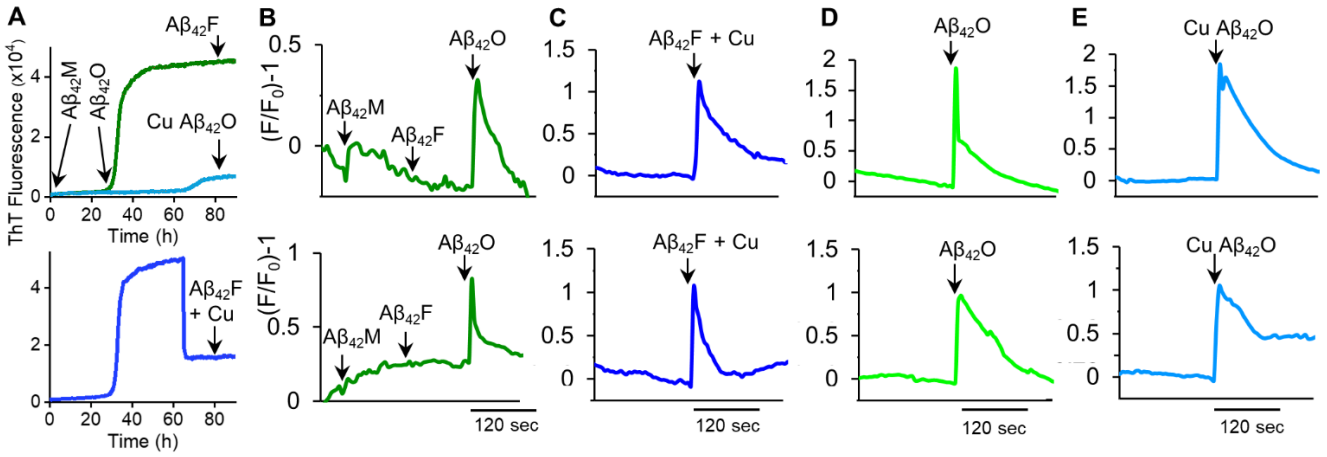

Figure 6: Calcium influx of HEK293T cells in response to different Aβ42 preparations. (A) ThT fibril growth curves indicating the five Aβ42 preparations used. HEK293T cells are loaded with Ca(II) sensitive fluorescent dye, Fluro3-AM. (B) Time-lapse recording of fluorescence relative to fluorescence before addition of Aβ42 monomer($Aβ_{42}M$), and subsequent addition of Aβ42 fibril($Aβ_{42}F$), Aβ42 oligomer($Aβ_{42}O$). Notably, only Aβ42 oligomers cause calcium influx. (C) Aβ42 fibril disassembled into oligomers, by Cu(II) addition, causes Ca(II) influx in HEK cells. (D) Aβ42 oligomers from the lag-phase causes Ca(II) influx. (E) Aβ42 assembly is trapped as oligomers by Cu(II) and causes Ca(II) influx. Aβ42 (5 μM) is added to extracellular media, buffered at pH 7.4.

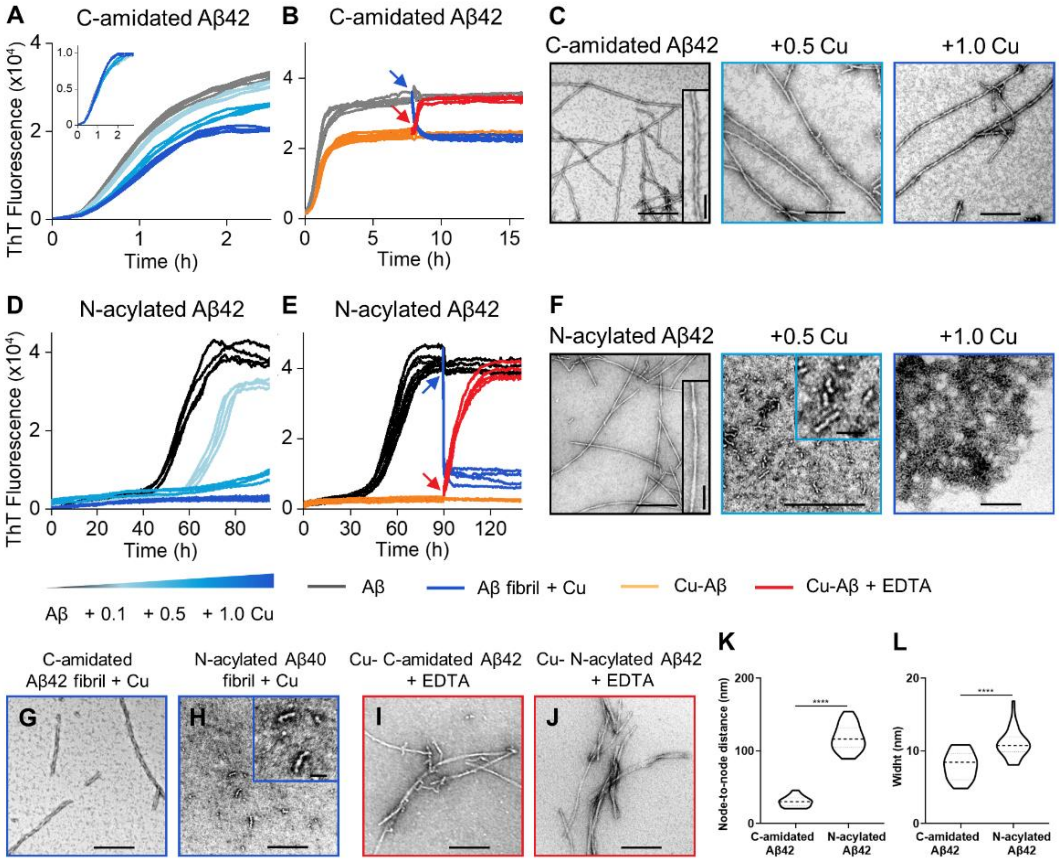

Figure 7: Cu(II) impact on C-amidated Aβ42 and N-acylated Aβ42 aggregation. Cu(II) has relatively little impact on C-amidated Aβ42 fibril formation, in contrast to wild-type Aβ42 and the N-terminal amidated Aβ42, which are trapped as oligomers by Cu(II). Kinetics profiles of 10 μM C-amidated Aβ42 (A) and N-acylated Aβ42 (D) in the absence and presence of 0.1, 0.5 and 1.0 molar equivalents of Cu^{2+}. Insert shows normalized ThT fluorescence. Kinetics profiles of 10 μM C-amidated Aβ42 (B) and N-acylated Aβ42 (E) in the absence (black/gray) and presence (orange) of 8 μM Cu^{2+}. 8 μM Cu^{2+} (blue) or 50 μM EDTA (red) was added to half the samples at 8 h for C-amidated Aβ42 and 90 h for N-acylated Aβ42. N = 4 traces for each condition. TEM fibril images produced at 0, 0.5 and 1.0 molar equivalents of Cu^{2+} for C-amidated Aβ42 (C) and N-acylated Aβ42 (F). TEM images of C-amidated Aβ42 (G) and N-acylated Aβ42 (H) produced with Cu^{2+} added to preformed fibrils. C-amidated Aβ42 (I) and N-acylated Aβ42 (J) in the presence of Cu^{2+} with subsequent EDTA addition. Scale bars: 200 nm; inset 30 nm. (K) Node-to-node distance of C-amidated Aβ42 and N-acylated Aβ42 fibril twists. (L) Fibril widths. N=50 individual fibrils are measured per condition.

Cu(II) and familial Aβ mutants - Arctic and Italian

There are several rare point mutations within Aβ that cluster at residues 22 or 23 and cause early onset familiar Alzheimer's disease.[76-77] We wondered if the mutated forms of Aβ might be influenced by Cu(II) differently from wild-type Aβ. These mutations are believed to effect the type of fibril fold, due to the loss of a colombic interaction between Asp23 and Lys28, observed for wild-type Aβ40.[78]

We have monitored fibril growth of the Arctic (E22G) and Italian (E22K) mutants, in the presence and absence of Cu(II) ions, for Aβ40 and Aβ42, Figure 8. Arctic Aβ40 and Italian Aβ40 behaves very differently from wild-type Aβ40. Rather than accelerate Aβ40 fibril formation (Figure 2A), Cu(II) has an impact on fibril formation similar to wild-type Aβ42. Both the ThT signal and TEM images show marked inhibition of fibril formation with sub-stochiometric Cu(II) addition, Figure 8. Cu(II) traps both Aβ40 and Aβ42 for both familial mutants as oligomers. Further TEM images showing Cu(II) trapping both Aβ40 and Aβ42 mutants as protofibrils for all four isoforms, are shown in Figure S9-S12. In support of this switch in behavior for the Aβ40 mutants, we have performed EDTA additions and Cu(II) addition to preformed fibrils, shown in Figure 9. Again, the behavior of Aβ40(Arctic) and Aβ40(Italian) mimics the behavior of wild-type Aβ42 in the presence of Cu(II). This data, Figure 9, confirms Cu(II) traps Aβ40 and Aβ42 Arctic and Italian as oligomers, these oligomers are capable of rapidly seeding fibril formation upon the removal of Cu(II) with EDTA.

The Glu22 (mutated to Gly or Lys in Arctic and Italian mutants respectively) does not directly coordinate within the Cu(II) complex, however there is a structural explanation for this switch in behavior. Many of the familial point mutations are situated at residue 22 and 23 and have been link with the formation of a salt-bridge to Lys28.[78] Molecular structures of Arctic Aβ40 fibrils indicates a basic 'S' shaped topology which is much closer to the appearance of longer wild-type Aβ42.[79-81] Indeed, we have recently shown that Arctic Aβ40 fibrils can cross-seed wild-type Aβ42 fibril formation, which suggests a very similar and compatible structure.[75] Similarly, Aβ40 Osaka familial mutant (E22Δ) has an 'S' shape arrangement similar to wild-type Aβ42.[82]

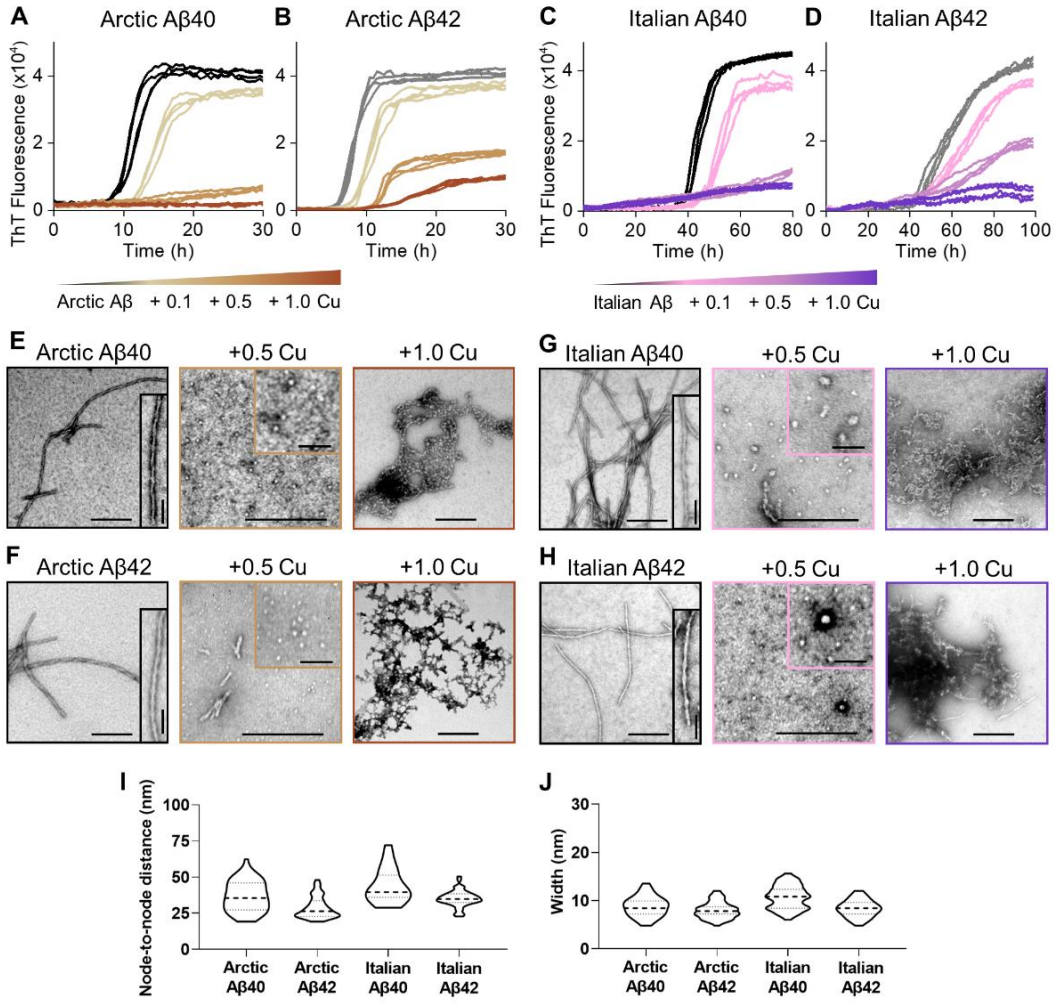

Figure 8: Cu^{2+} inhibits Arctic and Italian Aβ40 and Aβ42 fibril formation. Kinetics profiles of 10 μM Arctic Aβ40 (A), Arctic Aβ42 (B), Italian Aβ40 (C) and Italian Aβ42 (D) in the absence and presence of 0.1, 0.5 and 1.0 molar equivalents of Cu^{2+}. Negatively stained TEM fibril images produced at 0, 0.5 and 1.0 molar equivalents of Cu^{2+} for Arctic Aβ40 (E), Arctic Aβ42 (F), Italian Aβ40 (G) and Italian Aβ42 (H). Scale bars: 200 nm; inset 50 nm. (I) Node-to-node distance of fibril twists. (J) Fibril width. N=50 individual fibrils are measured per condition.

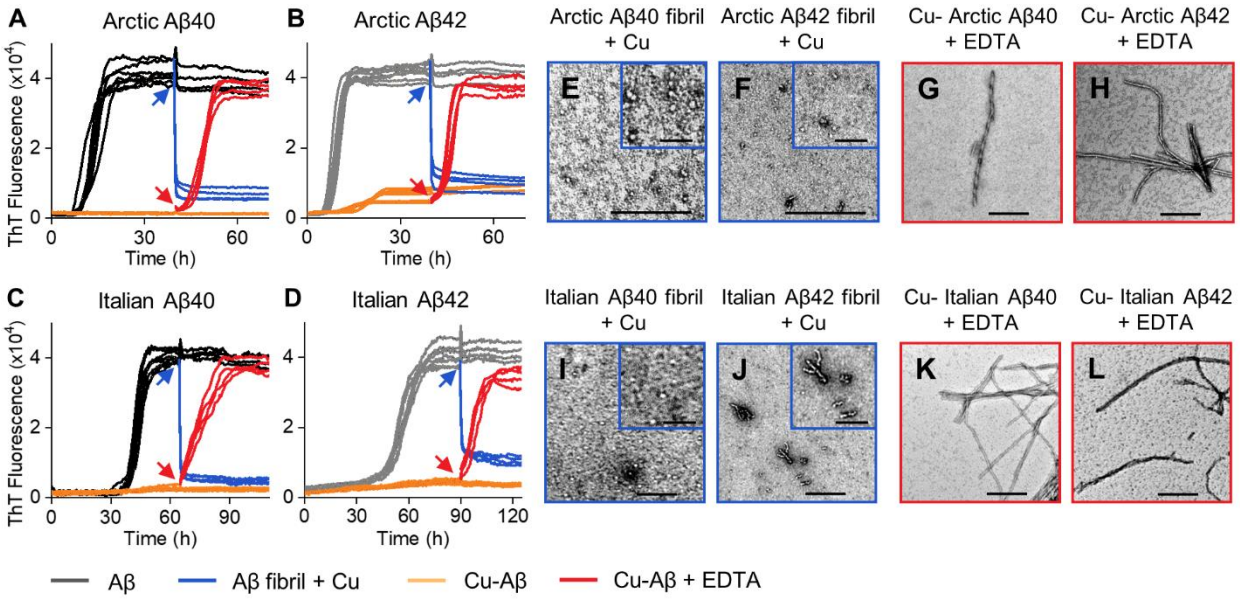

Figure 9: Switching on/off the fibril growth of Arctic Aβ and Italian Aβ by EDTA and Cu^{2+}. Kinetics profiles of 10 μM Arctic Aβ40 (A), Arctic Aβ42 (B), Italian Aβ40 (C) and Italian Aβ42 (D) in the absence (black/gray) and presence (orange) of 8 μM Cu^{2+}. 8 μM Cu^{2+} (blue) or 50 μM EDTA (red) was added to half the samples at 40 h for Arctic Aβ40/42, 65 h for Italian Aβ40 and 90 h for Italian Aβ42. Preparations were incubated with 20 μM ThT in 30 mM HEPES and 160 mM NaCl buffer (pH 7.4) at 30 °C quiescently. N = 4 traces for each condition. TEM images of Arctic Aβ40 (E), Arctic Aβ42 (F), Italian Aβ40 (I) and Italian Aβ42 (J) produced with Cu^{2+} added to preformed fibrils. Arctic Aβ40 (I), Arctic Aβ42 (J), Italian Aβ40 (K) and Italian Aβ42 (L) in the presence of Cu^{2+} with subsequent EDTA addition. Scale bars: 200 nm; inset 50 nm.

Furthermore, residues 22 and 23 are a 'hot-spot' for mutations associated with early on-set AD, consequently there is much interest in the turn formed at these residues, this has been explored by incorporation of a D-chiral center [83] or a lactam ring. [84]

As an aside from the Cu(II) loaded studies, we have also compaired the twist periodicity and fibril width, for the various isoforms studied including Arctic and Italian mutants, Figure 8I, J with that of wild-type Aβ, Figure 1D, E and also N- and C-blocked Aβ42 shown in Figure 7K, L, in the absence of Cu(II). It is notable that the shorter Aβ40 isofoms for wild-type and familial mutants tend to have a longer twist periodicity than the various Aβ42 fibrils, both wild-type and mutant. Related studies of fibril twist morphology for familial mutants have been reported.[85-86]

CONCLUSION

The differential Cu(II) induced fibril/oligomer formation for wild-type Aβ40 compared to the other Aβ isoforms has ramifications for Aβ toxicity *in vivo*. It has long been assumed that the heightened toxicity for wild-type Aβ42 and the familiar mutants is linked with elevated amyloidogenicity, relative to the non-pathogenic wild-type Aβ40. Here, we show an even more marked contrast in behaviour, which could be linked with Cu(II) trapping Aβ as oligomers for Aβ42 and the familiar mutants (such as Arctic Aβ40 and Italian Aβ40 mutants). *In vivo*, familial mutants of Aβ40 isoforms out-number Aβ42 in a 9-to-1 ratio.[87-88] Thus, for those with the Arctic or Italian mutation, physiological Cu(II) will trap the much more abundant Aβ40 (Arctic) or Aβ40 (Italian) as toxic oligomers. This will increase the level of Cu(II) trapped toxic oligomers nine-fold, relative to wild-type Aβ. This might explain why these particular mutations cause early onset AD. Our studies suggest Cu(II) chelation could conceivably be a therapeutic approach,[33] by reducing the amount of toxic oligomers present *in vivo*.

METHODS

Aβ Peptides

All Aβ peptides were purchased from EZBiolab Inc in a lyophilized form. Aβ peptides were synthesized using solid-phase F-moc (*N*- (9-fluorenyl)methoxycarbonyl) chemistry, and were purified with reverse-phase high performance liquid chromatography. The sequence was confirmed with mass spectrometry. The following amino acid sequences were generated:

Wild-type Aβ40: DAEFR HDSGY EVHHQ KLVFF AEDVG SNKGA IIGLM VGGVV

Wild-type Aβ42: DAEFR HDSGY EVHHQ KLVFF AEDVG SNKGA IIGLM VGGVV IA

Arctic Aβ40: DAEFR HDSGY EVHHQ KLVFF AGDVG SNKGA IIGLM VGGVV

Arctic Aβ42: DAEFR HDSGY EVHHQ KLVFF AGDVG SNKGA IIGLM VGGVV IA

Italian Aβ40: DAEFR HDSGY EVHHQ KLVFF AKDVG SNKGA IIGLM VGGVV

Italian Aβ42: DAEFR HDSGY EVHHQ KLVFF AKDVG SNKGA IIGLM VGGVV IA

N-terminally acylated: Aβ42:

D(acylated)AEFR HDSGY EVHHQ KLVFF AEDVG SNKGA IIGLM VGGVV IA

C-terminally amidated: Aβ42:

DAEFR HDSGY EVHHQ KLVFF AEDVG SNKGA IIGLM VGGVV IA(amidated)

Unless otherwise stated, all other chemicals were purchased from Sigma-Aldrich.

Monomeric Aβ by size-exclusion chromatography (SEC)

Aβ peptides were solubilized in ultra-high quality water to 0.7 mg ml^{-1} and adjusting to pH 10 with NaOH and left at 4 °C for 30 min. Then, samples were centrifuged for 10 min at 20,000 g at 4°C, to remove any high molecular weight aggregates. In order to generate a seed-free preparation, size-exclusion chromatography (SEC) was used to remove any remaining nucleating and oligomeric aggregates, see supplemental Figure S13. Monomeric Aβ was isolated by AKTA FPLC with a Superdex 75 10/300 GL column (volume = 24 ml; GE Healthcare) with a flow rate of 0.5 mL·min^{-1} at 4 °C. The column was pre-equilibrated with 30 mM 4-(2-hydroxyethyl)-1-piperazineethanesulfonic acid (HEPES), 160 mM NaCl buffer at pH 7.4. The Aβ peptides concentration were determined using tyrosine 10 absorption at 280 nm, ε_{280}=1280·cm^{-1} mol^{-1}. Negative-stain electron microscopy and thioflavin T fluorescence assay confirmed that SEC-purified Aβ peptides were seed-free. Monomeric Aβ were used directly after SEC elution.

SEC Fibril growth assay

The kinetics of amyloid fibril formation were monitored with thioflavin T (ThT), a dye which widely employed for monitoring amyloid fibril formation.[89] 10 μM monomeric Aβ peptides and 20 μM ThT were placed in a 96-well plate in 30 mM HEPES and 160 mM NaCl buffer at pH 7.4 at 30 °C. The well plate remained quiescent. ThT fluorescence was recorded using a FLUOstar Omega microplate reader (BMG Labtech, Aylesbury, UK), with excitation filters at 440 nm and emission filters at 490 nm. Kinetic assays in the presence of Cu^{2+} were performed under the same conditions. In the seeded aggregation assay, seeds (Aβ fibrils) 5%; 0.5 μM Aβ monomer equivalent, were obtained by incubating 10 μM Aβ peptides in 30 mM HEPES and 160 mM NaCl buffer at 30 °C for 5 days. The formation of Aβ fibrils was confirmed by ThT fluorescent assay and TEM imaging.

Fitting fibril growth curves

The empirical kinetic values for the time at which lag-times (t_{lag}, time required for the ThT fluorescence to reach 10% of the maximum value), half maximal fluorescence is reached (t_{50}) and transition time from 10% to 90% of the maximum value (t_{growth}) were extracted from the data by fitting the fibril growth curve to the following equation.[90]

$$Y = (y_i + m_i x) + \frac{v_f + m_f x}{1 + e^{-(\frac{x - x_0}{\tau})}}$$

Where Y represents the ThT fluorescence intensity, and x represents the time. x_o is the time at which half maximal ThT fluorescence is reached, referred to as t_{50}. The lag-time (t_{lag}) is taken from $t_{lag} = x_0 - 2\tau$. The initial and final fluorescence signals is represented by y_i and γ_f, respectively.[90]

Analysis of Aβ aggregation kinetics

AmyloFit online platform was used for the global kinetic analysis of amyloid formation.[67] The Aβ aggregation traces are described by the following integrated rate law, based on Michaelis-Menten-Like Kinetics:

$$\frac{M}{M(\infty)} = 1 - \left(1 - \frac{M(0)}{M(\infty)}\right) e^{-k_\infty t} \times \left(\frac{B_- + C_+ e^{\kappa t}}{B_+ + C_+ e^{\kappa t}} \times \frac{B_+ + C_+}{B_- + C_+}\right)^{\frac{K_\infty^2}{\overline{k}_\infty \kappa}}$$

where the additional coefficients are functions of κ and λ:

$$C_\pm = \frac{k_+[P]_0}{\kappa} \pm \frac{k_+ M(0)}{2m(0)k_+} \pm \frac{\lambda^2}{2\kappa^2}$$

$$k_\infty = 2k_+ P(\infty)$$

$$\overline{k}_\infty = \sqrt{k_\infty^2 - 2C_+ C_- \kappa^2}$$

$$\boldsymbol{B}_\pm = (\boldsymbol{k}_\infty \pm \overline{\boldsymbol{k}}_\infty)/2\boldsymbol{\kappa}$$

which are two combinations of the microscopic rate constants of:

$$\lambda = \sqrt{2k_+ k_n m(0)^{nc}}$$

$$\kappa = \sqrt{2m(0)k_+ \frac{m(0)^{n2} k_2}{1 + m(0)^{n2}/K_M}}$$

where $m(0)$ is the initial monomer concentration; $M(0)$, $P(0)$, $M(\infty)$ and $P(\infty)$ are the fibril mass concentration and fibril number concentration in the initial and at equilibrium of the aggregation, respectively. The microscopic rate constants for primary nucleation (k_n), secondary nucleation (k_2), and elongation rate (k_+). K_M is the saturation constant for secondary nucleation. The exponents n_c and n_2 are the reaction orders for primary and secondary nucleation, respectively.

Aβ fibril assembly was fitted to a secondary nucleation model.[91] The experimental macro kinetic traces were globally fitting to the integrated rate law over the range of Cu^{2+} concentrations. The microscopic rate constants k_n, k_+, and k_2 values were fitted to the Aβ fibril growth curves in the absence of Cu^{2+}. The other kinetic traces at increasing Cu^{2+} concentrations, were then fitted in three scenarios in which only one of the rate constants were permitted to vary, while the other two remain as single (globally fitted) constants. With the initial monomer concentration fixed as a global constant (10 μM), n_c and n_2 were set as global constant of 2 so as not over-fit the data. This approach has been used to study how increasing concentrations of an inhibitor of fibril formation effect individual micro-rate constants.[92-94]

Transmission electron microscopy

Aβ fibril samples were generated with the same protocol for Aβ fibril growth assay but without ThT addition. 5 μL aliquot of sample were added onto glow discharged 300-mesh carbon-coated copper grids (Agar Scientific Ltd) using the droplet method, with ddH_20 washes before and after addition of stain. Glow discharge was carried out by the EasiGlow glow discharge cleaning system (Pelco inc, USA). 5 μL uranyl acetate (2 % w/v) was used to negatively stain the samples, then blotted and rinsed after 10 seconds at room temperature. Imaging was carried out on a JEOL JEM-1230 electron microscope (JEOL, Ltd., Japan) at 80,000 magnifications, operated at 120 kV, paired with a 2k Morada CCD camera and corresponding microscope image analysis software (Olympus Europa, UK). Node-to-node fibril distance was measured by image-J software.

Cellular Ca(II) influx

Fluo3-AM loaded HEK293T cells: HEK293T cells were incubated at 37 °C, 5% CO2 incubator, in Dulbecco's modified Eagle's medium (DMEM, purchased from Thermofisher) supplemented with 10% fetal bovine serum and penicillin-streptomycin (0.2 mg/ml). Cells were plated into a 12-well plate, 1 mL each well, and incubated overnight, cells typically gained *ca*. 70% confluence. Next medium was replaced with fresh DMEM which was supplemented with 5 μM of Fluo3-AM (Abcam). To enable the cellular uptake of the Ca^{2+} sensitive fluorescent dye, plates were left in an incubator for a further 30 min. Excess extra-cellular Fluo3-AM was removed by two washes of 400 μL of DMEM Eagles cell medium in each well. Cells were then incubated for a further 20 minutes at 37 °C to allow de-esterification of intracellular Fluo-3 to occur, which activates Ca^{2+} dependent fluorescence. Finally, the DMEM was replaced with an aqueous buffer containing $CaCl_2$ (1.8 mM); NaCl (120 mM); CsCl (10 mM); HEPES (9 mM); KCl (2.2 mM); $MgCl_2$ (1.9 mM), buffered to pH 7.4. The Fluo-3 loaded cells were then ready for time-lapse fluorescence microscopy.

Ca^{2+} Fluorescence Imaging of Fluo-3: Fluorescence microscopy was performed using an inverted Leica DM IL microscope, with a magnification of 10x. The bandpass filter allowed excitation at 470 nm and emission was recorded at 520 nm. Time-lapse fluorescence images and bright-field visible light images were acquired using a charge-coupled device (CCD) camera with a temporal resolution of one image every 5 s, recordings were for 10 mins.

The microscope was operated using ProgRes CapturePro 2.8.8 software and fluorescence intensities were measured by analysing the total field (typically ca. 500 individual cells), using the time series analyser V3 plugin and Image-J. Changes in Fluo-3 fluorescence signals are presented as (F/F_0)-1, where (F) is the observed fluorescence and (F_0) is the background fluorescence at a time point just before the addition of Aβ. Typically, each condition was recorded using three separate wells, with independent repeats.

The impact of five Aβ42 preparations were studied, including: monomers (SEC purified); oligomers (from the end of the lag-phase); fibrils (from the plateau-phase); Cu(II) trapped oligomers; Cu(II) disassembled fibrils. Stock solutions of 30 μM Aβ was added to HEK293 cells within 400 μL of cell medium to produce a final Aβ (monomer equivalent) concentration of 5 μM.

ASSOCIATED CONTENT

Supporting Information

The Supporting Information is available free of charge at: http://pubs.acs.org. Table S1 of kinetic data, and Figures S1-S13 includes: TEM images of various Aβ assemblies with and without the presence of Cu^{2+}; ThT monitor fibril formation kinetics and chromatograms of SEC purified Aβ monomers.

Corresponding Author

John Viles – School of Biological and Behavioral Sciences, Queen Mary University of London, London, E1 4NS, United Kingdom. Email: j.viles@qmul.ac.uk

Authors

Yao Tian – School of Biological and Behavioral Sciences, Queen Mary University of London, London, E1 4NS, United Kingdom

Qi Shang – School of Biological and Behavioral Sciences, Queen Mary University of London, London, E1 4NS, United Kingdom

Ruina Liang – School of Biological and Behavioral Sciences, Queen Mary University of London, London, E1 4NS, United Kingdom

Author Contributions

All authors have given approval to the final version of the manuscript.

Funding Sources

BBSRC; project grant code BB/Y001931/1 and BB/M023877/1.

Notes

The authors declare no competing financial interest.

ACKNOWLEDGMENT

We are thankful for the support of the BBSRC; project grant code BB/Y001931/1 and BB/M023877/1 and Chinese Scholarship Council (CSC).

ABBREVIATIONS

AD, Alzheimer's disease; Aβ, amyloid-beta; ThT, thioflavin T; TEM, transmission electron microscopy; SEC, size exclusion chromatography.

REFERENCES

(1) Prince, M.; Bryce, R.; Albanese, E.; Wimo, A.; Ribeiro, W.; Ferri, C. P., The global prevalence of dementia: a systematic review and metaanalysis. *Alzheimers Dement* **2013,** *9* (1), 63-75 e2.
(2) Hardy, J. A.; Higgins, G. A., Alzheimer's disease: the amyloid cascade hypothesis. *Science* **1992,** *256* (5054), 184-185.
(3) Selkoe, D. J., The molecular pathology of Alzheimer's disease. *Neuron* **1991,** *6* (4), 487-498.
(4) Selkoe, D. J.; Hardy, J., The amyloid hypothesis of Alzheimer's disease at 25 years. *EMBO Mol. Med.* **2016,** *8* (6), 595-608.
(5) Naslund, J.; Schierhorn, A.; Hellman, U.; Lannfelt, L.; Roses, A. D.; Tjernberg, L. O.; Silberring, J.; Gandy, S. E.; Winblad, B.; Greengard, P.; et al., Relative abundance of Alzheimer A beta amyloid peptide variants in Alzheimer disease and normal aging. *Proc. Natl. Acad. Sci. U. S. A.* **1994,** *91* (18), 8378-82.
(6) Scheuner, D.; Eckman, C.; Jensen, M.; Song, X.; Citron, M.; Suzuki, N.; Bird, T. D.; Hardy, J.; Hutton, M., Kukull, W.; Larson, E.; Levy-Lahad, E.; Viitanen, M.; Peskind, E.; Poorkaj, P.; Schellenberg, G., Secreted amyloid beta-protein similar to that in the senile plaques of Alzheimer's disease is increased in vivo by the presenilin 1 and 2 and APP mutations linked to familial Alzheimer's disease. *Nat. Med.* **1996,** *2*, 864-870.
(7) Citron, M.; Westaway, D.; Xia, W.; Carlson, G.; Diehl, T.; Levesque, G.; Johnson-Wood, K.; Lee, M.; Seubert, P.; Davis, A.; Kholodenko, D.; Motter, R.; Sherrington, R.; Perry, B.; Yao, H.; Strome, R.; Lieberburg, I.; Rommens, J.; Kim, S.; Schenk, D.; Fraser, P.; St George Hyslop, P.; Selkoe, D. J., Mutant presenilins of Alzheimer's disease increase production of 42-residue amyloid beta-protein in both transfected cells and transgenic mice. *Nat. Med.* **1997,** *3* (1), 67-72.
(8) Duff, K.; Eckman, C.; Zehr, C.; Yu, X.; Prada, C. M.; Perez-tur, J.; Hutton, M.; Buee, L.; Harigaya, Y.; Yager, D.; Morgan, D.; Gordon, M. N.; Holcomb, L.; Refolo, L.; Zenk, B.; Hardy, J.; Younkin, S., Increased amyloid-β42(43) in brains of mice expressing mutant presenilin 1. *Nature* **1996,** *383* (6602), 710-713.
(9) Burdick, D.; Soreghan, B.; Kwon, M.; Kosmoski, J.; Knauer, M.; Henschen, A.; Yates, J.; Cotman, C.; Glabe, C., Assembly and

aggregation properties of synthetic Alzheimer's A4/beta amyloid peptide analogs. *J. Biol. Chem.* **1992,** *267* (1), 546-554.
(10) Lambert, M. P.; Barlow, A. K.; Chromy, B. A.; Edwards, C.; Freed, R.; Liosatos, M.; Morgan, T. E.; Rozovsky, I.; Trommer, B.; Viola, K. L.; Wals, P.; Zhang, C.; Finch, C. E.; Krafft, G. A.; Klein, W. L., Diffusible, nonfibrillar ligands derived from Aβ1-42 are potent central nervous system neurotoxins. *Proc. Natl. Acad. Sci. U. S. A.* **1998,** *95*, 6448-6453.
(11) Walsh, D. M.; Klyubin, I.; Fadeeva, J. V.; Cullen, W. K.; Anwyl, R.; Wolfe, M. S.; Rowan, M. J.; Selkoe, D. J., Naturally secreted oligomers of amyloid beta protein potently inhibit hippocampal long-term potentiation in vivo. *Nature* **2002,** *416*, 535-539.
(12) Lesné, S.; Koh, M. T.; Kotilinek, L.; Kayed, R.; Glabe, C. G.; Yang, A.; Gallagher, M.; Ashe, K. H., A specific amyloid-β protein assembly in the brain impairs memory. *Nature* **2006,** 440, 352-357.
(13) Yankner, B. A.; Lu, T., Amyloid β-protein toxicity and the pathogenesis of Alzheimer disease. *J. Biol. Chem.* **2009,** *284*, 4755-4759.
(14) Yasumoto, T.; Takamura, Y.; Tsuji, M.; Watanabe-Nakayama, T.; Imamura, K.; Inoue, H.; Nakamura, S.; Inoue, T.; Kimura, A.; Yano, S.; Nishijo, H.; Kiuchi, Y.; Teplow, D. B.; Ono, K., High molecular weight amyloid β(1-42) oligomers induce neurotoxicity via plasma membrane damage. *FASEB J*. **2019,** *33*, 9220-9234.
(15) Tian, Y.; Liang, R.; Kumar, A.; Szwedziak, P.; Viles, J. H., 3D-visualization of amyloid-beta oligomer interactions with lipid membranes by cryo-electron tomography. *Chem. Sci.* **2021,** *12*, 6896-6907.
(16) Bode, D. C.; Baker, M. D.; Viles, J. H., Ion Channel Formation by Amyloid-beta42 Oligomers but Not Amyloid-β40 in Cellular Membranes. *J. Biol. Chem.* **2017,** *292*, 1404-1413.
(17) Viles, J. H., Imaging Amyloid-beta Membrane Interactions: Ion-Channel Pores and Lipid-Bilayer Permeability in Alzheimer's Disease. *Angew. Chem. Int. Ed.* **2023**, e202215785.
(18) Viles, J. H., Metal ions and amyloid fiber formation in neurodegenerative diseases. Copper, zinc and iron in Alzheimer's, Parkinson's and prion diseases. *Coord. Chem. Rev.* **2012,** *256*, 2271-2284.
(19) Bush, A. I.; Pettingell, W. H.; Multhaup, G.; d Paradis, M.; Vonsattel, J. P.; Gusella, J. F.; Beyreuther, K.; Masters, C. L.; Tanzi, R. E., Rapid induction of Alzheimer Aβ amyloid formation by zinc. *Science* **1994,** *265*, 1464-1467.
(20) Atwood, C. S.; Moir, R. D.; Huang, X.; Scarpa, R. C.; Bacarra, N. M.; Romano, D. M.; Hartshorn, M. A.; Tanzi, R. E.; Bush, A. I., Dramatic aggregation of Alzheimer Aβ by Cu(II) is induced by conditions representing physiological acidosis. *J. Biol. Chem.* **1998,** *273*, 12817-12826.
(21) Cheignon, C.; Tomas, M.; Bonnefont-Rousselot, D.; Faller, P.; Hureau, C.; Collin, F., Oxidative stress and the amyloid beta peptide in Alzheimer's disease. *Redox Biol*. **2018,** *14*, 450-464.
(22) Gu, M.; Bode, D. C.; Viles, J. H., Copper Redox Cycling Inhibits Abeta Fibre Formation and Promotes Fibre Fragmentation, while Generating a Dityrosine Abeta Dimer. *Sci*. *Rep*. **2018,** *8*, 16190.
(23) Bagheri, S.; Squitti, R.; Haertle, T.; Siotto, M.; Saboury, A. A., Role of Copper in the Onset of Alzheimer's Disease Compared to Other Metals. *Front. Aging Neurosci.* **2017,** *9*, 446.
(24) James, S. A.; Volitakis, I.; Adlard, P. A.; Duce, J. A.; Masters, C. L.; Cherny, R. A.; Bush, A. I., Elevated labile Cu is associated with oxidative pathology in Alzheimer disease. *Free Radic. Biol. Med.* **2012,** *52*, 298-302.
(25) Li, D. D.; Zhang, W.; Wang, Z. Y.; Zhao, P., Serum Copper, Zinc, and Iron Levels in Patients with Alzheimer's Disease: A Meta-Analysis of Case-Control Studies. *Front Aging Neurosci.* **2017,** *9*, 300.
(26) Lovell, M. A.; Robertson, J. D.; Teesdale, W. J.; Campbell, J. L.; Markesbery, W. R., Copper, iron and zinc in Alzheimer's disease senile plaques. *J. Neurol. Sci.* **1998,** *18*, 47-52.
(27) Dong, J.; Atwood, C. S.; Anderson, V. E.; Siedlak, S. L.; Smith, M. A.; Perry, G.; Carey, P. R., Metal binding and oxidation of amyloid-beta within isolated senile plaque cores: Raman microscopic evidence. *Biochemistry* **2003,** *42* (10), 2768-2773.
(28) Miller, L. M.; Wang, Q.; Telivala, T. P.; Smith, R. J.; Lanzirotti, A.; Miklossy, J., Synchrotron-based infrared and X-ray imaging shows focalized accumulation of Cu and Zn co-localized with beta-amyloid deposits in Alzheimer's disease. *J. Struct. Biol.* **2006,** *155*, 30-37.
(29) Sanokawa-Akakura, R.; Cao, W.; Allan, K.; Patel, K.; Ganesh, A.; Heiman, G.; Burke, R.; Kemp, F. W.; Bogden, J. D.; Camakaris, J.; Birge, R. B.; Konsolaki, M., Control of Alzheimer's amyloid beta toxicity by the high molecular weight immunophilin FKBP52 and copper homeostasis in Drosophila. *PLoS One* **2010,** *5*, e8626.
(30) Singh, S. K.; Sinha, P.; Mishra, L.; Srikrishna, S., Neuroprotective Role of a Novel Copper Chelator against Aβ 42 Induced Neurotoxicity. *Int. J. Alzheimers Dis.* **2013,** *2013*, 567128.
(31) Sparks, D. L.; Schreurs, B. G., Trace amounts of copper in water induce beta-amyloid plaques and learning deficits in a rabbit model of Alzheimer's disease. *Proc. Natl. Acad. Sci. U. S. A.* **2003,** *100*, 11065-11069.
(32) Matlack, K. E.; Tardiff, D. F.; Narayan, P.; Hamamichi, S.; Caldwell, K. A.; Caldwell, G. A.; Lindquist, S., Clioquinol promotes the degradation of metal-dependent amyloid-β (Aβ) oligomers to restore endocytosis and ameliorate Abeta toxicity. *Proc. Natl. Acad. Sci. U. S. A.* **2014,** *111*, 4013-4018.
(33) Cherny, R. A.; Atwood, C. S.; Xilinas, M. E.; Gray, D. N.; Jones, W. D.; McLean, C. A.; Barnham, K. J.; Volitakis, I.; Fraser, F. W.; Kim, Y.; Huang, X.; Goldstein, L. E.; Moir, R. D.; Lim, J. T.; Beyreuther, K.; Zheng, H.; Tanzi, R. E.; Masters, C. L.; Bush, A. I., Treatment with a copper-zinc chelator markedly and rapidly inhibits β-amyloid accumulation in Alzheimer's disease transgenic mice. *Neuron* **2001,** *30*, 665-676.
(34) Prana, Prana Biotechnology announces top line results of Phase 2 IMAGINE trial of PBT2 in Alzheimer's disease. *Alzheimer's disease, Investor Announcement* **2014**, *1*,1-36 .
(35) Sarell, C. J.; Syme, C. D.; Rigby, S. E.; Viles, J. H., Copper(II) binding to amyloid-beta fibrils of Alzheimer's disease reveals a picomolar affinity: stoichiometry and coordination geometry are independent of Aβ oligomeric form. *Biochemistry* **2009,** *48*, 4388-4402.
(36) Seubert, P.; Vigo-Pelfrey, C.; Esch, F.; Lee, M.; Dovey, H.; Davis, D.; Sinha, S.; Schlossmacher, M.; Whaley, J.; Swindlehurst, C.; et al., Isolation and quantification of soluble Alzheimer's β-peptide from biological fluids. *Nature* **1992,** *359*, 325-327.
(37) Kardos, J.; Kovács, I.; Hajós, F.; Kálmán, M.; Simonyi, M., Nerve endings from rat brain tissue release copper upon depolarization. A possible role in regulating neuronal excitability. *Neurosci. Lett.* **1989,** *103*, 139-144.
(38) Hartter, D. E.; Barnea, A., Evidence for release of copper in the brain: depolarization-induced release of newly taken-up 67copper. *Synapse* **1988,** *2*, 412-415.
(39) Faller, P.; Hureau, C., Bioinorganic chemistry of copper and zinc ions coordinated to amyloid-β peptide. *Dalton Trans.* **2009,**7, 1080-94.
(40) Karr, J. W.; Szalai, V. A., Cu(II) binding to monomeric, oligomeric, and fibrillar forms of the Alzheimer's disease amyloid-β peptide. *Biochemistry* **2008,** *47*, 5006-5016.
(41) Syme, C. D.; Nadal, R. C.; Rigby, S. E.; Viles, J. H., Copper binding to the amyloid-β (Aβ) peptide associated with Alzheimer's disease: folding, coordination geometry, pH dependence, stoichiometry, and affinity of Abeta-(1-28): insights from a range of complementary spectroscopic techniques. *J. Biol. Chem.* **2004,** *279*, 18169-77.
(42) Dorlet, P.; Gambarelli, S.; Faller, P.; Hureau, C., Pulse EPR spectroscopy reveals the coordination sphere of copper(II) ions in the 1-16 amyloid-β peptide: a key role of the first two N-terminus residues. *Angew. Chem. Int. Ed.* **2009,** *48*, 9273-9276.
(43) Shin, B. K.; Saxena, S., Substantial contribution of the two imidazole rings of the His13-His14 dyad to Cu(II) binding in amyloid-β(1-16) at physiological pH and its significance. *J. Phys. Chem. A.* **2011,** *115*, 9590-9602.
(44) Drew, S. C.; Noble, C. J.; Masters, C. L.; Hanson, G. R.; Barnham, K. J., Pleomorphic copper coordination by Alzheimer's disease amyloid-β peptide. *J. Am. Chem. Soc.* **2009,** *131*, 1195-1207.
(45) Parthasarathy, S.; Long, F.; Miller, Y.; Xiao, Y.; McElheny, D.; Thurber, K.; Ma, B.; Nussinov, R.; Ishii, Y., Molecular-level examination of Cu^{2+} binding structure for amyloid fibrils of 40-residue Alzheimer's β by solid-state NMR spectroscopy. *J. Am. Chem. Soc.* **2011,** *133*, 3390-3400.

(46) Gunderson, W. A.; Hernandez-Guzman, J.; Karr, J. W.; Sun, L.; Szalai, V. A.; Warncke, K., Local structure and global patterning of Cu^{2+} binding in fibrillar amyloid-β [Aβ(1-40)] protein. *J. Am. Chem. Soc.* **2012,** *134*, 18330-18337.
(47) Jun, S.; Gillespie, J. R.; Shin, B. K.; Saxena, S., The second Cu(II)-binding site in a proton-rich environment interferes with the aggregation of amyloid-β(1-40) into amyloid fibrils. *Biochemistry* **2009,** *48*, 10724-10732.
(48) Matheou, C. J.; Younan, N. D.; Viles, J. H., Cu^{2+} accentuates distinct misfolding of Aβ(1-40) and Aβ(1-42) peptides, and potentiates membrane disruption. *Biochem. J.* **2015,** *466*, 233-242.
(49) Tougu, V.; Karafin, A.; Zovo, K.; Chung, R. S.; Howells, C.; West, A. K.; Palumaa, P., Zn(II)- and Cu(II)-induced non-fibrillar aggregates of amyloid-β(1-42) peptide are transformed to amyloid fibrils, both spontaneously and under the influence of metal chelators. *J. Neurochem.* **2009,** *110*, 1784-1795.
(50) Sharma, A. K.; Pavlova, S. T.; Kim, J.; Kim, J.; Mirica, L. M., The effect of Cu^{2+} and Zn^{2+} on the Abeta42 peptide aggregation and cellular toxicity. *Metallomics* **2013,** *5*, 1529-1536.
(51) Sarell, C. J.; Wilkinson, S. R.; Viles, J. H., Substoichiometric levels of Cu2+ ions accelerate the kinetics of fiber formation and promote cell toxicity of amyloid-β from Alzheimer disease. *J. Biol. Chem.* **2010,** *285*, 41533-41540.
(52) Pedersen, J. T.; Ostergaard, J.; Rozlosnik, N.; Gammelgaard, B.; Heegaard, N. H., Cu(II) mediates kinetically distinct, non-amyloidogenic aggregation of amyloid-β peptides. *J. Biol. Chem.* **2011,** *286*, 26952-26963.
(53) Abelein, A.; Ciofi-Baffoni, S.; Morman, C.; Kumar, R.; Giachetti, A.; Piccioli, M.; Biverstal, H., Molecular Structure of Cu(II)-Bound Amyloid-beta Monomer Implicated in Inhibition of Peptide Self-Assembly in Alzheimer's Disease. *JACS Au* **2022,** *2*, 2571-2584.
(54) Crooks, E. J.; Irizarry, B. A.; Ziliox, M.; Kawakami, T.; Victor, T.; Xu, F.; Hojo, H.; Chiu, K.; Simmerling, C.; Van Nostrand, W. E.; Smith, S. O.; Miller, L. M., Copper stabilizes antiparallel β-sheet fibrils of the amyloid-β40 (Aβ40)-Iowa variant. *J. Biol. Chem.* **2020,** *295*, 8914-8927.
(55) Somavarapu, A. K.; Shen, F.; Teilum, K.; Zhang, J.; Mossin, S.; Thulstrup, P. W.; Bjerrum, M. J.; Tiwari, M. K.; Szunyogh, D.; Sotofte, P. M.; Kepp, K. P.; Hemmingsen, L., The Pathogenic A2V Mutant Exhibits Distinct Aggregation Kinetics, Metal Site Structure, and Metal Exchange of the Cu^{2+}-Aβ Complex. *Chemistry* **2017,** *23*, 13591-13595.
(56) Chen, W. T.; Hong, C. J.; Lin, Y. T.; Chang, W. H.; Huang, H. T.; Liao, J. Y.; Chang, Y. J.; Hsieh, Y. F.; Cheng, C. Y.; Liu, H. C.; Chen, Y. R.; Cheng, I. H., Amyloid-β (Aβ) D7H mutation increases oligomeric Abeta42 and alters properties of Abeta-zinc/copper assemblies. *PLoS One* **2012,** *7*, e35807.
(57) Danielsson, J.; Pierattelli, R.; Banci, L.; Gräslund, A., High-resolution NMR studies of the zinc-binding site of the Alzheimer's amyloid beta-peptide. *FEBS J.* **2007**, 274, 46-59.
(58) Syme, C. D.; Viles, J. H., Solution 1H NMR investigation of Zn2+ and Cd^{2+} binding to amyloid-β peptide (Aβ) of Alzheimer's disease. *Biochim. Biophys. Acta.* **2006,** *1764*, 246-256.
(59) Mekmouche, Y.; Coppel, Y.; Hochgrafe, K.; Guilloreau, L.; Tallmard, C.; Mazarguil, H.; Faller, P., Characterization of the Zn-II binding to the peptide amyloid-beta(1-16) linked to Alzheimer's disease. *Chembiochem.* **2005,** *6*, 1663-1671.
(60) Abelein, A.; Graslund, A.; Danielsson, J., Zinc as chaperone-mimicking agent for retardation of amyloid beta peptide fibril formation. *Proc. Natl. Acad. Sci. U. S. A.* **2015,** 112, 5407-5412.
(61) Silva, K. I.; Saxena, S., Zn(II) Ions Substantially Perturb Cu(II) Ion Coordination in Amyloid-β at Physiological pH. *J. Phys. Chem. B* **2013,** *117*, 9386-9394.
(62) Matheou, C. J.; Younan, N. D.; Viles, J. H., The Rapid Exchange of Zinc Enables Trace Levels to Profoundly Influence Amyloid-β Misfolding and Dominates Assembly Outcomes in Cu/Zn Mixtures. *J. Mol. Bio.* **2016,** *428*, 2832-2846.
(63) Lutter, L.; Aubrey, L. D.; Xue, W. F., On the Structural Diversity and Individuality of Polymorphic Amyloid Protein Assemblies. *J. Mol. Biol.* **2021,** *433*, 167124.
(64) Meinhardt, J.; Sachse, C.; Hortschansky, P.; Grigorieff, N.; Fandrich, M., Aβ(1-40) fibril polymorphism implies diverse interaction patterns in amyloid fibrils. *J. Mol. Biol.* **2009,** *386*, 869-877.
(65) Dahlgren, K. N.; Manelli, A. M.; Stine, W. B., Jr.; Baker, L. K.; Krafft, G. A.; LaDu, M. J., Oligomeric and fibrillar species of amyloid-β peptides differentially affect neuronal viability. *J. Biol. Chem.* **2002,** *277*, 32046-32053.
(66) Benilova, I.; Karran, E.; De Strooper, B., The toxic Aβ oligomer and Alzheimer's disease: an emperor in need of clothes. *Nat. Neurosci.* **2012,** *15*, 349-357.
(67) Meisl, G.; Kirkegaard, J. B.; Arosio, P.; Michaels, T. C.; Vendruscolo, M.; Dobson, C. M.; Linse, S.; Knowles, T. P., Molecular mechanisms of protein aggregation from global fitting of kinetic models. *Nat. Protoc.* **2016,** *1*, 252-272.
(68) Tian, Y.; Viles, J. H., pH Dependence of Amyloid-β Fibril Assembly Kinetics: Unravelling the Microscopic Molecular Processes. *Angew. Chem. Int. Ed.* **2022,** *61*, e202210675.
(69) Xiao, Y.; Ma, B.; McElheny, D.; Parthasarathy, S.; Long, F.; Hoshi, M.; Nussinov, R.; Ishii, Y., Abeta(1-42) fibril structure illuminates self-recognition and replication of amyloid in Alzheimer's disease. *Nat. Struct. Mol. Biol.* **2015,** *22*, 499-505.
(70) Paravastu, A. K.; Leapman, R. D.; Yau, W. M.; Tycko, R., Molecular structural basis for polymorphism in Alzheimer's β-amyloid fibrils. *Proc. Natl. Acad. Sci. U. S. A.* **2008,** *105*, 18349-18354.
(71) Gremer, L.; Scholzel, D.; Schenk, C.; Reinartz, E.; Labahn, J.; Ravelli, R. B. G.; Tusche, M.; Lopez-Iglesias, C.; Hoyer, W.; Heise, H.; Willbold, D.; Schroder, G. F., Fibril structure of amyloid-β(1-42) by cryo-electron microscopy. *Science* **2017,** *358*, 116-119.
(72) Ghosh, U.; Thurber, K. R.; Yau, W. M.; Tycko, R., Molecular structure of a prevalent amyloid-β fibril polymorph from Alzheimer's disease brain tissue. *Proc. Natl. Acad. Sci. U. S. A.* **2021,** *118*, e2023089118.
(73) Qiang, W.; Yau, W. M.; Lu, J. X.; Collinge, J.; Tycko, R., Structural variation in amyloid-β fibrils from Alzheimer's disease clinical subtypes. *Nature* **2017,** *541*, 217-221.
(74) Yang, Y.; Arseni, D.; Zhang, W.; Huang, M.; Lovestam, S.; Schweighauser, M.; Kotecha, A.; Murzin, A. G.; Peak-Chew, S. Y.; Macdonald, J.; Lavenir, I.; Garringer, H. J.; Gelpi, E.; Newell, K. L.; Kovacs, G. G.; Vidal, R.; Ghetti, B.; Ryskeldi-Falcon, B.; Scheres, S. H. W.; Goedert, M., Cryo-EM structures of amyloid-β 42 filaments from human brains. *Science* **2022,** *375*, 167-172.
(75) Liang, R.; Tian, Y.; Viles, J. H., Cross-seeding of WT amyloid-β with Arctic but not Italian familial mutants accelerates fibril formation in Alzheimer's disease. *J. Biol. Chem.* **2022,** *298*, 102071.
(76) Selkoe, D. J., Amyloid β-protein and the genetics of Alzheimer's disease. *J. Biol. Chem.* **1996,** *271*, 18295-18298.
(77) Cacace, R.; Sleegers, K.; Van Broeckhoven, C., Molecular genetics of early-onset Alzheimer's disease revisited. *Alzheimers Dement.* **2016,** *12*, 733-748.
(78) Schledorn, M.; Meier, B. H.; Bockmann, A., Alternative salt bridge formation in Aβ - a hallmark of early-onset Alzheimer's disease? *Front. Mol. Biosci.* **2015,** *2*, 14.
(79) Elkins, M. R.; Wang, T.; Nick, M.; Jo, H.; Lemmin, T.; Prusiner, S. B.; DeGrado, W. F.; Stohr, J.; Hong, M., Structural Polymorphism of Alzheimer's beta-Amyloid Fibrils as Controlled by an E22 Switch: A Solid-State NMR Study. *J. Am. Chem. Soc.* **2016,** *138*, 9840-9852.
(80) Yoo, B. K.; Xiao, Y.; McElheny, D.; Ishii, Y., E22G Pathogenic Mutation of β-Amyloid (Aβ) Enhances Misfolding of Abeta40 by Unexpected Prion-like Cross Talk between Aβ42 and Aβ40. *J. Am. Chem. Soc.* **2018,** *140*, 2781-2784.
(81) Yang, Y.; Zhang, W.; Murzin, A. G.; Schweighauser, M.; Huang, M.; Lovestam, S.; Peak-Chew, S. Y.; Saito, T.; Saido, T. C.; Macdonald, J.; Lavenir, I.; Ghetti, B.; Graff, C.; Kumar, A.; Nordberg, A.; Goedert, M.; Scheres, S. H. W., Cryo-EM structures of amyloid-β filaments with the Arctic mutation (E22G) from human and mouse brains. *Acta. Neuropathol* **2023,** *145*, 325-333.
(82) Schutz, A. K.; Vagt, T.; Huber, M.; Ovchinnikova, O. Y.; Cadalbert, R.; Wall, J.; Guntert, P.; Bockmann, A.; Glockshuber, R.; Meier, B. H., Atomic-resolution three-dimensional structure of amyloid β fibrils bearing the Osaka mutation. *Angew. Chem. Int. Ed.* **2015,** *54*, 331-335.
(83) Warner, C. J. A.; Dutta, S.; Foley, A. R.; Raskatov, J. A.,

Introduction of D-Glutamate at a Critical Residue of Aβ42 Stabilizes a Prefibrillary Aggregate with Enhanced Toxicity. *Chem-Eur. J.* **2016,** *22*, 11967-11970.
(84) Masuda, Y.; Uemura, S.; Ohashi, R.; Nakanishi, A.; Takegoshi, K.; Shimizu, T.; Shirasawa, T.; Irie, K., Identification of physiological and toxic conformations in Aβ42 aggregates. *Chembiochem* **2009,** *10*, 287-295.
(85) Hatami, A.; Monjazeb, S.; Milton, S.; Glabe, C. G., Familial Alzheimer's Disease Mutations within the Amyloid Precursor Protein Alter the Aggregation and Conformation of the Amyloid-β Peptide. *J. Biol. Chem.* **2017,** *292*, 3172-3185.
(86) Yang, X.; Meisl, G.; Frohm, B.; Thulin, E.; Knowles, T. P. J.; Linse, S., On the role of sidechain size and charge in the aggregation of Aβ42 with familial mutations. *Proc. Natl. Acad. Sci. U. S. A.* **2018,** *115*, E5849-E5858.
(87) Hellstrom-Lindahl, E.; Viitanen, M.; Marutle, A., Comparison of Abeta levels in the brain of familial and sporadic Alzheimer's disease. *Neurochem. Int.* **2009,** *55* 243-252.
(88) Kuperstein, I.; Broersen, K.; Benilova, I.; Rozenski, J.; Jonckheere, W.; Debulpaep, M.; Vandersteen, A.; Segers-Nolten, I.; Van Der Werf, K.; Subramaniam, V.; Braeken, D.; Callewaert, G.; Bartic, C.; D'Hooge, R.; Martins, I. C.; Rousseau, F.; Schymkowitz, J.; De Strooper, B., Neurotoxicity of Alzheimer's disease Abeta peptides is induced by small changes in the Aβ42 to Aβ40 ratio. *EMBO J.* **2010,** *29* 3408-3420.
(89) Younan, N. D.; Viles, J. H., A Comparison of Three Fluorophores for the Detection of Amyloid Fibers and Prefibrillar Oligomeric Assemblies. ThT (Thioflavin T); ANS (1-Anilinonaphthalene-8-sulfonic Acid); and bisANS (4,4'-Dianilino-1,1'-binaphthyl-5,5'-disulfonic Acid). *Biochemistry* **2015,** *54*, 4297-4306.
(90) Uversky, V. N.; Li, J.; Fink, A. L., Metal-triggered structural transformations, aggregation, and fibrillation of human alpha-synuclein. A possible molecular NK between Parkinson's disease and heavy metal exposure. *J. Biol. Chem.* **2001,** *276*, 44284-44296.
(91) Cohen, S. I.; Linse, S.; Luheshi, L. M.; Hellstrand, E.; White, D. A.; Rajah, L.; Otzen, D. E.; Vendruscolo, M.; Dobson, C. M.; Knowles, T. P., Proliferation of amyloid-β42 aggregates occurs through a secondary nucleation mechanism. *Proc. Natl. Acad. Sci. U. S. A.* **2013,** *110*, 9758-9763.
(92) Tian, Y.; Liu, J.; Yang, F.; Lian, C.; Zhang, H.; Viles, J. H.; Li, Z., Therapeutic potential for amyloid surface inhibitor: only amyloid-β oligomers formed by secondary nucleation disrupt lipid membrane integrity. *FEBS J.* **2022,** 289, 6767-6781.
(93) Cohen, S. I. A.; Arosio, P.; Presto, J.; Kurudenkandy, F. R.; Biverstal, H.; Dolfe, L.; Dunning, C.; Yang, X.; Frohm, B.; Vendruscolo, M.; Johansson, J.; Dobson, C. M.; Fisahn, A.; Knowles, T. P. J.; Linse, S., A molecular chaperone breaks the catalytic cycle that generates toxic Abeta oligomers. *Nat. Struct. Mol. Biol.* **2015,** *22*, 207-213.
(94) Aprile, F. A.; Sormanni, P.; Perni, M.; Arosio, P.; Linse, S.; Knowles, T. P. J.; Dobson, C. M.; Vendruscolo, M., Selective targeting of primary and secondary nucleation pathways in Aβ42 aggregation using a rational antibody scanning method. *Sci. Adv.* **2017,** *3*, e1700488.

Table of Contents artwork: